Geomechanics and Engineering, *Vol. 43, No. 1 (2025) 59-68*
https://doi.org/10.12989/gae.2025.43.1.059

Quantifying the uniformity of granular mixtures through a study on small-strain stiffness via DEM

Jian Gong[1], Jingwen Xu[1], Dianhong Huang[1], Yu Tang[1] and Zhiyong Liu*[2]

[1]*School of Civil Engineering and Architecture, Guangxi University, Nanning, Guangxi 530004, China*
[2]*Shanghai Key Laboratory of Rail Infrastructure Durability and System Safety, Tongji University, Shanghai 201804, China*

(*Received July 22, 2025, Revised September 27, 2025, Accepted September 29, 2025*)

Abstract. The conventional uniformity coefficient C_u fails to capture the uniformity of gap-graded granular mixtures. To address this limitation, this study introduces a new index C_u^m for quantifying mixture uniformity based on their small-strain stiffness G_0. Granular mixtures with varying fines content (FC) and particle size ratio (PSR) were prepared, and their G_0 values were determined through quasistatic drained triaxial tests. The corresponding C_u^m values were then derived from the measured G_0 values and expressed as a function of FC and PSR. The rationality of the proposed C_u^m was verified, and it was further demonstrated that C_u^m can be used to predict the small-strain stiffness of granular mixtures when the mechanical coordination number (CN_m), particle shear modulus of particles (G_p), confining stress (σ_0) and C_u^m are known.

Keywords: DEM; fines content; granular mixtures; particle size ratio; small-strain stiffness; uniformity coefficient

1. Introduction

The uniformity coefficient C_u is a commonly used parameter for characterizing the uniformity of continuous particle size distributions. In general, a larger C_u indicates a broader particle size distribution. As one of the fundamental soil properties, C_u plays a significant role in various geotechnical problems, including landslide erodibility (e.g., Chang *et al.* 2011), soil deformation (e.g., Sefi and Lav 2023, Do *et al*. 2024) and liquefaction (e.g., Monkul *et al.* 2021, Banerjee *et al*. 2023). Conventionally, C_u is determined as the ratio d_{60}/d_{10} from sieve analysis, where d_{60} and d_{10} represent the particle sizes corresponding to 60% and 10% passing by weight, respectively. The definition of C_u is suitable for continuously graded soils, but it may not applicable to gap-graded granular mixtures for two main reasons. First, for mixtures with specific fines content (FC), such as FC=10% and 60%, the particle size distribution exhibits a distinct gap, making it impossible to determine the characteristic diameters d_{60} and d_{10}. Without these characteristic particle sizes, the calculation of C_u is not feasible in these cases. For other FCs without such gaps, C_u can still be calculated. Second, the fundamental assumption of C_u is that a broader particle size span generally improves packing efficiency, as smaller particles fill the voids between larger ones. Thus, it is expected that the void ratio e decreases as C_u increases (Youd 1972). However, as shown in Fig. 1, which presents the relationships between maximum (e_{max}) and minimum (e_{min}) void ratios and for sand-silt mixtures (data from Polito and Martin 2001), both e_{max} and e_{min} exhibit three distinct stages: decreasing, plateau, and increasing. This observation contradicts the expectation of a continuous decrease with increasing C_u, further illustrating that the traditional C_u fails to adequately characterize the uniformity of gap-graded mixtures

Granular mixtures are gap-graded and have been verified that they are easy to suffer liquefaction failure under earthquake, specifically at the low fines content (FC) (e.g., Polito and Martin 2001, Thevanayagam *et al.* 2002). Soil stiffness takes a maximum value at very small strain levels (i.e., $<10^{-5}$), denoted as G_0 in the case of shear stiffness, is one of the fundamental properties of soil and plays a vital role in a variety of geotechnical problems. The typical application of G_0 is to evaluate the liquefaction potential. Accordingly, numerous experimental and numerical studies have focused on the G_0 of granular mixtures at the low FC (FC≤20%) (e.g., Chen *et al*. 2020, Gong *et al*. 2019, Goudarzy *et al.* 2016, Papadopoulou and Tika 2008, Rahman and Undrained 2014, Wang *et al*. 2022, Wei and Yang 2014, Wei and Yang 2019, Yang and Liu 2016, Zuo *et al*. 2023). Recently, some studies (e.g., Cheng *et al*. 2019, Shin 2018, Zhu *et al*. 2020) have paid attention to the higher FC. Besides the FC, the particle size ratio (PSR), indicating the size ratio between coarse particle and fines, is also an important factor for granular mixtures (e.g., Thevanayagam *et al.* 2002, Choo and Burns 2015, Yilmaz *et al.* 2023). Granular mixtures with different FC and PSR essentially indicate the different particle size distributions. Traditionally, the continuous particle size distribution can mainly be represented by the mean particle size d_{50} and uniformity coefficient C_u. Indeed, many previous experimental tests and numerical simulations have studied the effects of d_{50} and C_u on the G_0 of granular materials (e.g., Gu *et al.* 2017, Liu *et al.* 2023, Liu *et al.* 2021, Wichtmann and Triantafyllidis 2009). In summary, these studies found that the G_0 values remain nearly unchanged

*Corresponding author, Ph.D.
E-mail: zhiyongliu@tongji.edu.cn

ISSN: 2005-307X (Print), 2092-6219 (Online)

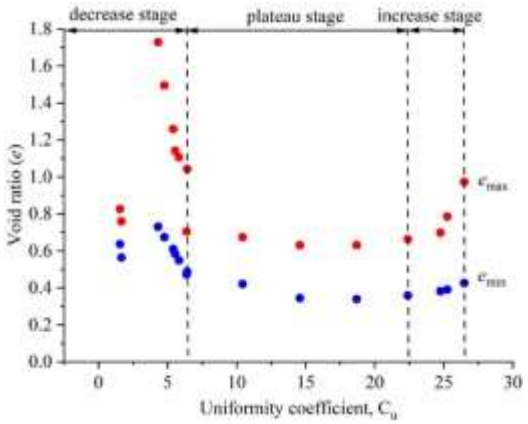

Fig. 1 Relationships between e_{max}, e_{min} and C_u for sand-silt mixtures (data adapted from Polito and Martin 2001)

with d_{50}, whereas G_0 values gradually decrease with an increase of C_u. Therefore, it is natural to associate that the effects of FC and PSR to essentially influence the uniformity to affect the G_0 of granular mixtures. Recently, Gong *et al.* (2024) reported that C_u actually reflects the uniformity distribution feature of contact stiffness inside the particle sample to affect the G_0 value. Furthermore, on the basis of discrete element method (DEM) simulations, Gong *et al*. (2024) proposed an empirical expression to predict G_0 value from a microscale perspective

$$G_0/{\sigma_0}^{1/3} = (19.08\mathrm{CN_m} - 66.72)$$
$$(22.54{G_\mathrm{p}}^{0.67} + 21.05)/[236.2(1.22 - 0.17\mathrm{C_u})] \quad (1)$$

where G_p is the shear modulus of particles; CN_m indicates the mechanical coordination number of granular materials (e.g., Thornton 2000). However, the Eq. (1) is only suitable for the continuous grading since the concept of C_u is possibly not applicable to the gap-graded granular mixtures as previously mentioned. Given these observations, a basic question naturally arises: is there an index for granular mixtures (C_u^m) to quantify their uniformity, and whether the C_u^m can be expressed as a function of FC and PSR? Furthermore, if the C_u^m exists, whether the G_0 of granular mixtures can be predicted by the Eq. (1) after replacing the C_u^m with C_u? These questions are the motivation of this work, wherein we conducted grain-scale modelling via the DEM, which has been demonstrated to be able to reproduce certain key features of granular materials (e.g., Gong *et al.* 2019, Gu and Yang 2013, Gu *et al*. 2020; Nei *et al*. 2022, Otsubo *et al*. 2020, Ostubo and O'Sullivan 2018, Zhao *et al*. 2023).

This paper aims to proposea new index C_u^m, that can be expressed of FC and PSR, to quantify the uniformity of granular mixtures. Three-dimensional (3D) DEM simulations are conducted to investigate the effects of FC and PSR on the G_0 of granular mixtures. The G_0 of the samples are determined by quasistatic drained triaxial tests. The remainder of this paper is organized as follows. DEM modelling is introduced first, followed by a series of macroscale and microscale analyses of the simulation results. Attempts are made to study the underlying mechanisms related to the variation in G_0 with FC and PSR.

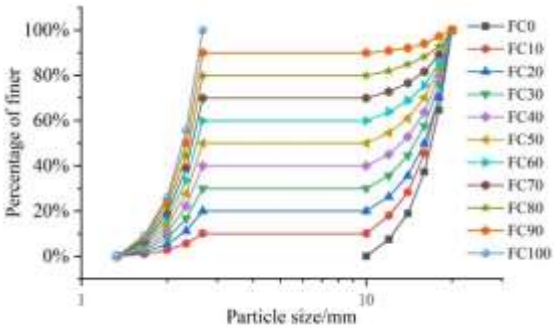

Fig. 2 Particle size distribution curves of granular mixtures with different FCs (PSR = 7.5)

Then, an index of uniformity coefficient for granular mixtures C_u^m is proposed. Afterwards, the rationality of the proposed C_u^m is verified. Finally, some primary conclusions are summarized.

2. DEM modelling

The well-recognized commercial software PFC3D 5.0 (e.g., Itasca 2014) is used to perform the numerical simulations in this work. The fines content (FC) and particle size ratio (PSR) are two important parameters for granular mixtures when considering particle size distribution in DEM modelling. According to crystallography, a fine particle can exactly fill the void created by four tangent coarse particles with an identical diameter at PSR= 4.45 (e.g., Krishna and Pandey 1981). Considering that PSR= 4.45 is a threshold value, thereby, PSR=2.0, 3.0, 4.45, 6.0, and 7.5 are employed in this work. The average diameter of coarse particles is D_c=15.0 mm for different PSRs. Accordingly, the average diameters of fines are D_f=7.5, 5.0, 3.37, 2.5, and 2.0 mm, respectively. The diameters of coarse particles and fines are evenly distributed within the ranges of [2/3D_c, 4/3D_c] and [2/3D_f, 4/3D_f], respectively. The C_u values of pure coarse particles (C_{uc}) and fines (C_{uf}) are 1.429 and 1.412, respectively. The FC is varied from 0% to 100% at intervals of 10%. Fig. 2 shows an example of the particle size distributions of granular mixtures for different FCs at PSR = 7.5. It is worthy noting that the absolute particle size adopted in this study (D_c=15.0 mm) does not represent the actual physical scale of soil particles, but rather a numerical choice to balance computational efficiency with the need to capture the effects of gradation. Since DEM analyses primarily depend on FC and PSR, the findings remain applicable regardless of the absolute size of the particles.

Following previous DEM simulations (e.g., Gong *et al.* 2019, Gong *et al*. 2024, Zheng *et al.* 2025), the samples were generated using the isotropic compression method. First, coarse particles and fines were randomly placed within a cubic domain bounded by six rigid walls. Because the initially generated particles overlap significantly, the resulting contact forces are excessively large, causing particle-wall penetration. To address this, particle velocities and angular velocities were reset every 10 steps up 20000 steps. The assembly was then isotropic compressed, with a

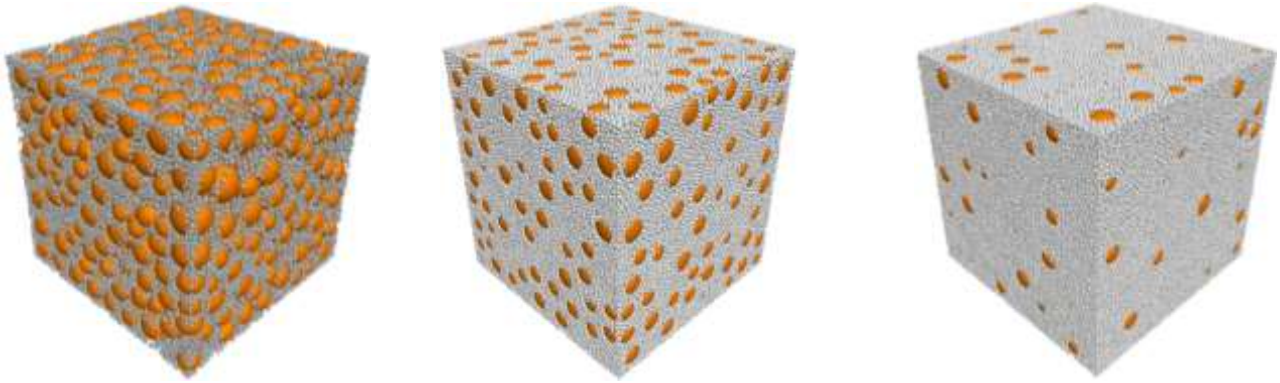

(a) FC=10% and PSR=7.5 (b) FC=30% and PSR=7.5 (c) FC=60% and PSR=7.5

Fig. 3 Typical numerical specimens with different FCs after reaching equilibrium

servo-control mechanism applied to reach the target confining stress of σ_0=200 kPa. Equilibrium was assumed once the ratio of the average unbalanced force to the average contact force fell below 1.0×10^{-5} and the deviation of the wall stress from 200 kPa was within 0.1%. Typical equilibrated specimens are shown in Fig. 3. Because frictionless particles were used during sample preparation, the densest packing was obtained. Accordingly, all samples in this study are considered to have an identical relative density of D_r=100%, following Azema and Radjai (2010, 2013). After isotropic compression, the samples were subjected to a drained triaxial test at very small strain, analogous to laboratory experiments. At such strain levels, the granular materials are generally considered to remain in an elastic state. Since contact sliding can cause particle rearrangement and lead to irreversible deformation, it was restricted in this study, consistent with the approach adopted by Gu *et al*. (2017). A small axial strain increment $\Delta\varepsilon_1$ was applied, while the lateral stress σ_2 (=σ_0) and σ_3 (=σ_0) were maintained constant using servo control until the shear strain $\gamma = \Delta\varepsilon_1 - 0.5(\Delta\varepsilon_2 + \Delta\varepsilon_3)$ reached 1.0×10^{-5}, where $\Delta\varepsilon_2$ and $\Delta\varepsilon_3$ denote the lateral strain increments. The small-strain stiffness G_0 was then determined by $G_0 = \Delta\sigma_1/2\gamma$, where $\Delta\sigma_1$ represents the axial stress increment.

In this study, granular mixtures can be regarded as sand-gravel mixtures due to ignoring the cohesion between particles. As reported by Gu *et al.* (2013), the linear contact law cannot reflect stress-dependent small-strain stiffness. Therefore, a nonlinear Hertz-Mindlin contact law is used to capture the force-dependent contact stiffness and thus stress-dependent small-strain stiffness. The main input microscale parameters used in our DEM simulations are summarized in Table 1. Among these, the particle material properties-particle density ρ=2650 kg/m^3, shear modulus G_p=29 GPa and Poisson's ratio ν_p = 0.15-are employed with reference to the experimentally determined values for Leighton Buzzard sand (e.g., Sandeep and Senetakis 2018, 2019). These parameters have also been widely employed in previous DEM simulations investigating the small-strain stiffness of granular materials (e.g., Gong *et al*. 2019, Gu *et al.* 2017, Liu *et al*. 2023, Gong *et al*. 2024, Gu and Yang 2013, Goudarzy *et al.* 2020, Gu and Yang 2018). A local damping factor of 0.7 is adopted to accelerate the process of reaching quasistatic equilibrium by dissipating the kinetic energy (e.g., Abbireddy and Clayton 2010). It is remarkable that the local damping can only weaken the accelerating forces and has a negligible influence on the fabric evolution at the small strain stage (e.g., Wang and Yan 2012).

Table 1 Input microscale parameters in the DEM simulations

Parameter	Values
Particle density, ρ (kg/m^3)	2650
Shear modulus, G_p (GPa)	29
Poisson's ratio, ν_p	0.15
Inter-particle frictional coefficient, μ	0.0

3. Results and discussion

3.1 Effects of FC and PSR

To quantify the effects of fines content (FC) and particle size ratio (PSR) on the small-strain stiffness G_0, Fig. 4 displays the relationship between G_0 (in MPa) and FC for the granular mixtures with different PSRs. As we can see, the evolutions of G_0 with FC follow the similar development for different PSRs. Specifically, with an increase of FC, G_0 first decreases and reaches a valley at FC=20%, then reversely increases and reaches a peak at a specific FC, and finally continuously decreases until FC=100%. The valley and peak G_0 are obviously affected by the PSRs and show a positive correlation with PSR.

Namely, the valley G_0 decreases and the peak G_0 increases with an increase of PSR. It is remarkable that the first decrease and then reversely increase of G_0 at low to medium FC is consistent with the observation in previous experimental studies (e.g., Goudarzy *et al.* 2016, Shin 2018). Furthermore, it can be observed that for the pure coarse particles (FC=0%) and fines (FC=100%) with different PSRs, their G_0 values are nearly the same. This finding indicates the particle size has limited effect on the G_0 values, which also has been demonstrated in previous experimental and DEM studies (e.g., Gu *et al*. 2017, Gu *et al.* 2020, Dutta *et al*. 2019). These observations suggest that the results of DEM simulations in this work are convincing.

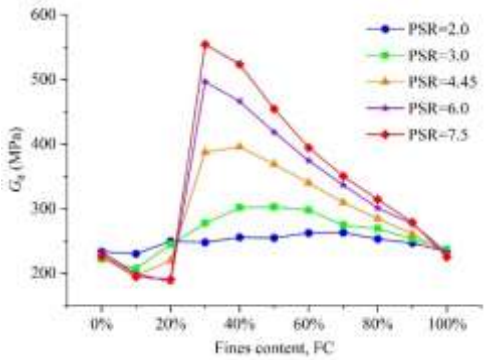

Fig. 4 The relationship between G_0 (in MPa) and FC for the granular mixtures with different PSRs

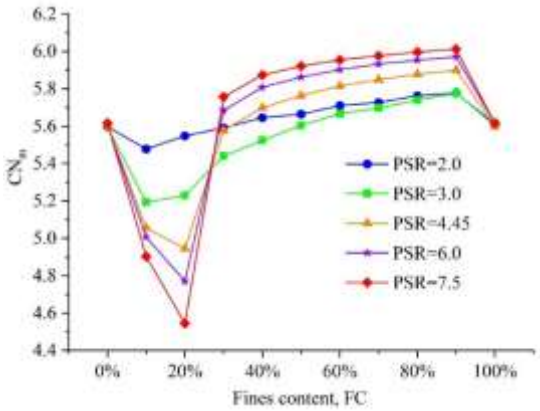

Fig. 5 The relationship between CN_m and FC for granular mixtures with different PSRs

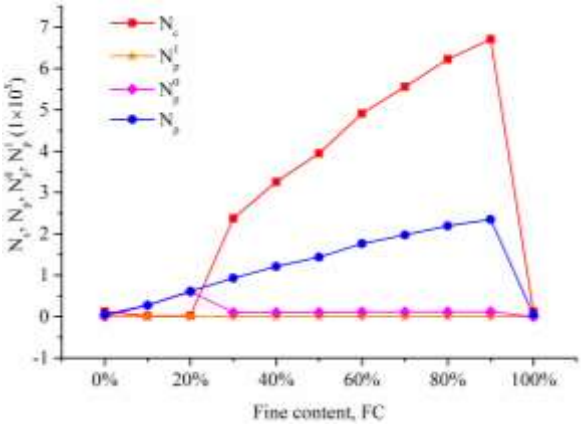

Fig. 6 The relationship between particle (N_p, N_p^0 and N_p^1), contact number (N_c) and FC for PSR=7.5

From the perspective of micromechanics, Gong *et al.* (2024) reported that the G_0 values are dependent on two microscale variants, i.e., the mechanical coordination number CN_m and contact stiffness between particles. Here, the contact stiffness between particles has two implications. One is the shear modulus of particles G_p. The other is the non-uniform distribution feature of contact stiffness inside the particle specimen. The effects of FC and PSR on the CN_m are first analyzed since many factors influencing on G_0, such as over-consolidation (e.g., Gu and Yang 2018), depositional fabric (e.g., Gong *et al.* 2019), and particle shape (e.g., Gong *et al.* 2024, Nei *et al.* 2022), are essentially related to the CN_m. Following Thornton (2000), CN_m in this work has eliminated the effect of rattlers. Specifically, CN_m is calculated as

$$CN_m = \frac{2N_c - N_p^1}{N_p - (N_p^0 + N_p^1)} \quad (2)$$

where N_c denotes the number of total contacts, N_p indicates the number of particles, N_p^0 refers to the number of particles without any contact, and N_p^1 represents the number of particles with only one contact. Remarkably, the contacts between particle and wall are not counted to avoid the boundary effect on CN_m (e.g., Pinson *et al.* 1998). Fig. 5 shows the relationships between CN_m and FC for the granular mixtures with different PSRs. It is clear that for PSRs ranging from 2.0 to 7.5, curves all exhibit a valley when FC≈20%, then reversely increases and reaches a peak at FC=90%, and finally decreases until FC=100%. The trends of the curves are consistent with the results in the literatures (e.g., Gong *et al.* 2021, Kristiansen *et al.* 2005, Meng *et al.* 2014). As the PSR increases, the valley locus moves rightward at FC=20%, which can be attributed to the smaller size of fines are rattlers and can move in the skeleton structure formed by coarse particles (e.g., Meng *et al.* 2014). When FC>20% at a specific FC, CN_m first decreases when PSR increases from 2.0 to 3.0, and then gradually increases with a further increase of PSR. The CN_m decreases with increasing FC when FC≤20% exhibits the similar trend with that of G_0 as shown in Fig. 4. Nevertheless, when FC>20%, the CN_m does not have an obvious peak at medium FC, which shows a different trend from that of G_0 as indicated in Fig. 4. To elucidate the evolution of CN_m with FC, the relationship between particle numbers (N_p, N_p^0 and N_p^1), contact number (N_c) and FC for PSR=7.5 is illustrated in Fig. 6. As shown, when FC⩽20%, $N_p^1 \approx 0$, $N_p \approx N_p^0$, and both of N_p and N_p^0 gradually increase with increasing FC. This indicates that most particles remain in a floating state within the specimens, leading to a near-zero contact number (N_c), as evidenced in Fig. 6. When FC>20%, both N_p^0 and N_p^1 approach zero, suggesting that floating particles become rare, while N_c and N_p progressively increase with FC. According to Eq. (2), because both the numerator and denominator simultaneously approach zero, this explains why the trend of CN_m with FC differs between the cases of FC⩽20% and FC>20%, as shown in Fig. 5.

To establish the relationship between G_0 and CN_m, Fig. 7 illustrates the relationship between $G_0/\sigma_0^{1/3}$ (G_0 in MPa and σ_0 in kPa) and CN_m for granular mixtures with different PSRs. We find that the data are scattered and $G_0/\sigma_0^{1/3}$ exhibits an obvious nonlinear trend with CN_m. This finding is different from the linear relationship between $G_0/\sigma_0^{1/3}$ and CN_m as reported in previous studies (e.g., Gong *et al.* 2024, Nei *et al.* 2022, Gu and Yang 2018, Gong *et al.* 2021). Considering that G_p=29 GPa is identical for all particles, the scattered data and nonlinear relationship between $G_0/\sigma_0^{1/3}$

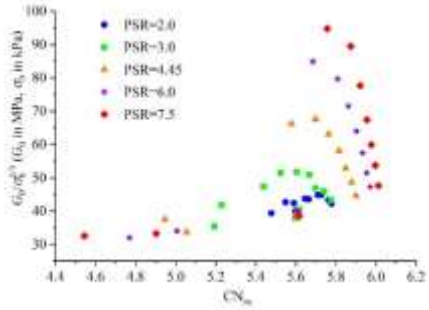

Fig. 7 The relationship between $G_0/\sigma_0^{1/3}$ and CN_m for granular mixtures with different PSRs

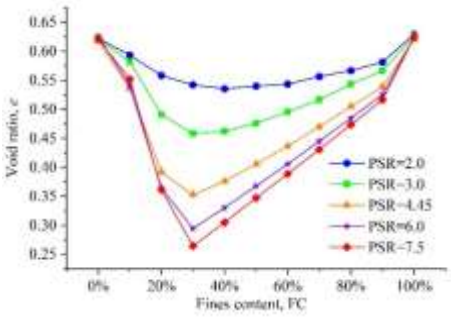

Fig. 8 Evolutions of e with FC for granular mixtures with different PSRs

and CN_m can be related to the non-uniform distribution feature of contact stiffness inside the particle samples. Gong *et al.* (2024) reported that non-uniform distribution feature of contact stiffness can be reflected by the C_u for the continuous grading when considering the contact stiffness on G_0. However, as previously mentioned in the introduction, the traditional definition of C_u possibly cannot reflect the uniformity of granular mixtures. Therefore, a new uniformity coefficient of granular mixtures should be proposed.

3.2 Uniformity coefficient of granular mixtures

We expect that the void ratio *e* has a negative correlation with the uniformity coefficient of granular mixtures C_u^m. Fig. 8 plots the evolutions of *e* with FC for granular mixtures with different PSRs. The five types of PSRs show a trend in which *e* first decreases, reaching a minimum value at a specific FC, and then reversely increases with increasing FC. As we can see, the PSR has an obvious influence on the minimum value of *e* and the FC corresponds to the *e* at their minimum value. Generally, the greater the PSR is, the minimum *e* is. Furthermore, the FC, corresponding to the *e* values at their minimum values, decreases with an increase of PSR. Specifically, for PSR=7.5, the *e* reaches the minimum value at FC≈30%, while for PSR=2.0, the *e* reaches the minimum value at FC≈50%. The same PSR effect on the evolutions of *e* with FC has also been found in previous studies (e.g., Yilmaz *et al.* 2023, Meng *et al.* 2014). It is interesting to point out that the FC, corresponding to the *e* values at their minimum values, is nearly the same with the G_0 values reach their

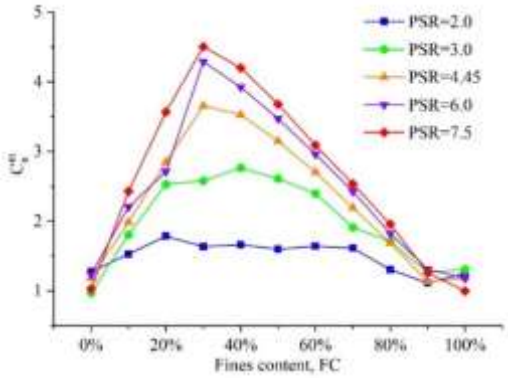

Fig. 9 The relationships between C_u^m and FC for granular mixtures with different PSRs

peaks as shown in Fig. 4. This finding suggests that the G_0 values have a potential correlation with e, possibly the C_u^m serve as the linking. According to the expectation of negative correlation between C_u^m and *e*, it infers that the C_u^m will show a unimodal characteristic with increasing FC. Furthermore, with an increase of PSR, the peak C_u^m will gradually increase, and the FC corresponding to the peak C_u^m will generally decrease.

Gong *et al.* (2024) proposed an empirical expression (Eq. (1)) to predict G_0 value from a microscale perspective. Note that the Eq. (1) includes the C_u to consider the non-uniformity distribution feature of contact stiffness inside the particle sample for the continuous grading. We assume that the Eq. (1) is also suitable for predicting the G_0 value for granular mixtures after replacing the C_u with C_u^m, then the Eq. (1) can be modified as follows.

$$G_0/{\sigma_0}^{1/3} = (19.08CN_m - 66.72)$$
$$(22.54{G_p}^{0.67} + 21.05)/[236.2(1.22 - 0.17C_u^m)] \quad (3)$$

Note that the unit of G_0, σ_0, and G_p are in MPa, kPa and GPa, respectively. In this work, σ_0=200 kPa and G_p=29 GPa are given for all the samples, while CN_m and C_u^m are changed for various FCs and PSRs. The measured G0 and CN_m for different FCs and PSRs are given in Figs. 4 and 5, respectively. Taking the C_u^m as the unique unknown quantity, the Eq. (3) can be written as follows.

$$C_u^m = 7.18 - (19.08CN_m - 66.72)$$
$$(22.54{G_p}^{0.67} + 21.05){\sigma_0}^{1/3}/(40.20G_0) \quad (4)$$

Substituting σ_0=200 kPa and G_p=29 GPa into the Eq. (4), then we have

$$C_u^m = 7.18 - 34.40(19.08CN_m - 66.72)/G_0 \quad (5)$$

Note that the Eq. (5) is sustainable for the given σ_0=200 kPa and G_p=29 GPa in this study, the expression is different for other values of σ_0 and G_p. After substituting the G_0 and CN_m of various FCs and PSRs into the Eq. (5), the C_u^m for various FCs and PSRs can be obtained. Fig. 9 illustrates the relationships between C_u^m and FC for granular mixtures with different PSRs. As we can see, the evolutions of C_u^m with FC for different PSRs fulfilled all the anticipations. That is,

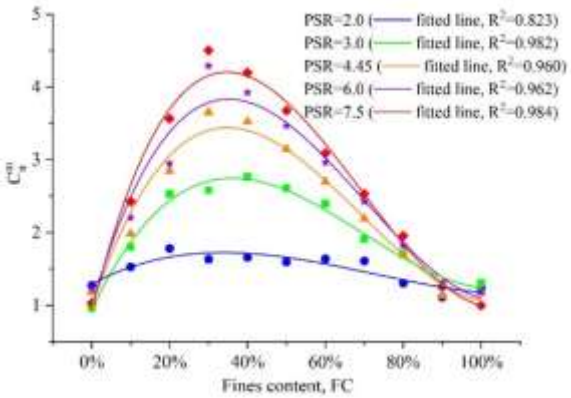

Fig. 10 The fitted lines of C_u^m with FC for granular mixtures with different PSRs

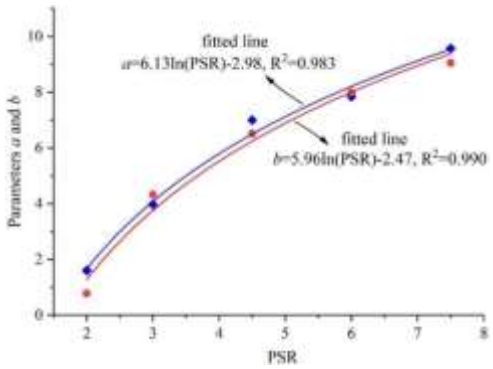

Fig. 11 The fitted relationships between a, b and PSR based on data in Table 2

Table 2 The fitted parameters a and b

PSR	2.0	3.0	4.45	6.0	7.5
a	1.60	3.97	7.00	7.84	9.57
b	0.78	4.33	6.51	8.00	9.05

on the one hand, all curves exhibit a unimodal characteristic with increasing FC and the peak C_u^m gradually increases with an increase of PSR. On the other hand, the FC corresponding to the peak C_u^m generally decreases with an increase of PSR.

It is found that the evolutions of C_u^m (Fig. 9) and e (Fig. 8) are generally similar and asymmetric about the horizontal axis. To fit the evolutions of C_u^m with FC, the similar fitting equation referring to the evolutions of e can be used. Yu and Standish (1988) proposed a two-parameter model to fit the relationship between e and FC as follows.

$$e = 2\gamma FC^3 - (3\gamma + \beta)FC^2 + (\gamma + \beta + e_f - e_c)FC + e_c \quad (6)$$

where e_f and e_c represent the void ratio of pure fines and coarse particles, respectively; γ and β are two fitting parameters. According to the Eq. (6), the similar fitting equation referring to the evolutions of C_u^m with FC can be expressed as follows.

$$C_u^m = 2aFC^3 - (3a + b)FC^2 + (a + b + C_{uf} - C_{uc})FC + C_{uc} \quad (7)$$

where C_{uf} and C_{uc} represent the C_u of pure fines and coarse particles, respectively; and a and b are two fitted parameters. Eq. (7) ensures that the obtained C_u^m equals to conventional C_u for the boundary granular mixtures, i.e., C_{uc} for FC=0% and C_{uf} for the FC=100%. Moreover, Eq. (7) indicates that the C_u^m of granular mixtures is independent of specimen density, even though the results in this study were derived from specimens prepared at the densest state. This observation aligns with the intuitive understanding that the coefficient of uniformity of granular materials is unrelated to density state, primarily because Eq. (7) is essentially derived from Eq. (1). Gong *et al.* (2024) further confirmed that Eq. (1) can be applied to reliably predict the small-strain stiffness of specimens across different density states. Fig. 10 illustrates the data points of C_u^m and their fitted lines by using the Eq. (7) for granular mixtures with different PSRs. It is remarkable that C_{uf}=1.412 and C_{uc}=1.429 are fixed when fitting the data points. The fitted parameters a and b are listed in Table 2. As we can see, it is evident that the data points can well be fitted by the Eq. (7). All R^2 values are generally greater than 0.89 except R^2=0.823 for PSD=2.0.

Reviewing the Eq. (7), when C_{uf} and C_{uc} values are specific, the C_u^m of granular mixtures can be determined when the parameters a and b are given. Fig. 11 plots the fitted relationships between a, b and PSR based on data in Table 2. It is evident that both the a and b are logarithms relationship with PSR. Specifically, the a~PSR and b~PSR relationships can be fitted as follows.

$$a = 6.13ln(\text{PSR}) - 2.98 \quad (8)$$

$$b = 5.96ln(\text{PSR}) - 2.47 \quad (9)$$

According to the Eqs. (7)-(9), the C_u^m of granular mixtures then can be calculated for a given PSR, FC, C_{uf} and C_{uc}. After the C_u^m is obtained, the G_0 values then can be calculated based on the Eq. (3) from a microscale perspective.

To examine the reasonability of the obtained C_u^m, the triaxial tests on granular mixtures with PSR=9.0 are conducted. The FC is varied from 0% to 100% at intervals of 10%. The sample preparation and microscale parameters are the same with that introduced in the section of DEM modelling. Specifically, D_c=15.0 mm, D_f=1.67 mm, C_{uf}=1.412 and C_{uc}=1.429. After substituting PSR=9.0 into the Eq. (8) and Eq. (9), the parameters a and b are obtained. Then, based on the Eq. (7), the value of C_u^m can be calculated for the different FCs. Afterwards, substituting C_u^m, CN_m into the Eq. (3) (G_p=29 GPa and σ_0=200 kPa), the G_0 of different FCs can be predicted. Fig. 12 compares the evolutions of the measured $G_0/\sigma_0^{1/3}$ and predicted $G_0/\sigma_0^{1/3}$ with FC. The inset shows the relationship between the measured $G_0/\sigma_0^{1/3}$ and predicted $G_0/\sigma_0^{1/3}$. The R^2 is used to analyses the scatter in the results. It is clear that the evolution of measured $G_0/\sigma_0^{1/3}$ with FC is generally consistent with that of predicted $G_0/\sigma_0^{1/3}$. the R^2=0.936 also suggests that the prediction of $G_0/\sigma_0^{1/3}$ compares well with

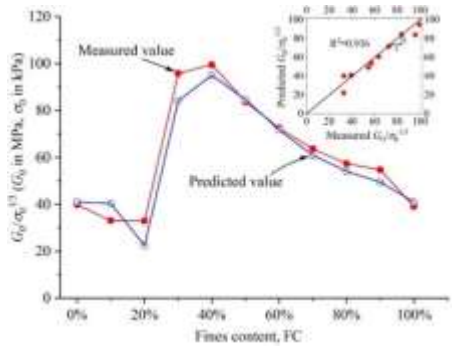

Fig. 12 Comparison between measured and predicted values of $G_0/\sigma_0^{1/3}$

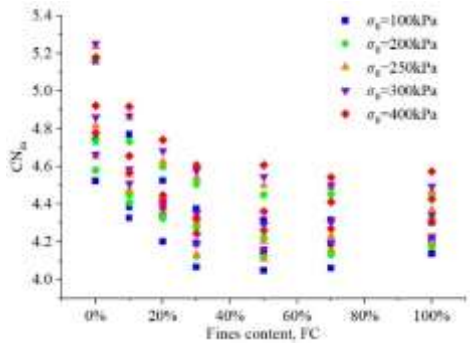

Fig. 13 The experimental data in Ruan *et al.* (2021).

the measured values. In addition, the laboratory experimental data in Ruan *et al.* (2021) is also plotted in Fig. 13 to further examine the reasonability of the obtained C_u^m. Notably, the small stiffness G_0 was measured and the CN_m cannot be obtained from the laboratory experiments, thus we will compare whether the value of CN_m obtained based on the Eqs. (3) and (7)-(9) is reasonable. As shown in Fig. 13, the value of CN_m falls in a typical range of 4.0~6.0, which is consistent with the findings in our study and previous researches (e.g., Yang and Liu 2016, Gong *et al.* 2019, Liu *et al.* 2024). These findings directly and indirectly demonstrate that the obtained C_u^m is reasonable and can be used to accurately predict the G_0 of granular mixtures.

As illustrated in Fig. 1, the traditional definition of C_u cannot fulfill the expectation that the void ratios of granular mixtures e will continuously decrease with an increase of C_u. To further check the reasonability of the obtained C_u^m, the relationship between the e values and C_u^m is studied. Fig. 14 presents the variation of e of granular mixtures with different FCs and PSRs with C_u^m. Note that the data in Gong *et al.* (2024) for the continuous grading are also included for comparison, in which the horizontal axis represents the C_u. As we can see, for both continuous grading and gap-graded granular mixtures, the measured e monotonically decreases with an increase of C_u^m and C_u as expected. Furthermore, at a given C_u^m for granular mixtures and C_u for continuous grading, the e values are generally scattered. Nevertheless, the difference between the e values for granular mixtures and that for continuous grading are not obvious. Therefore, it concludes that the obtained C_u^m for the gap-graded granular mixtures has the same meaning as

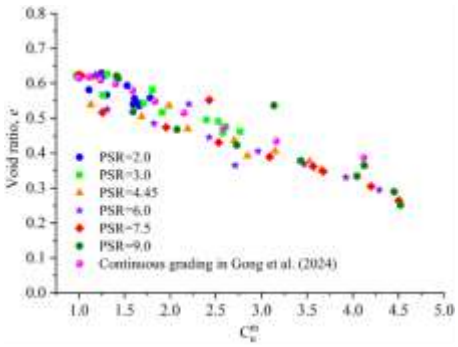

Fig. 14 Variation of e with C_u^m for granular mixtures with different FCs and PSRs

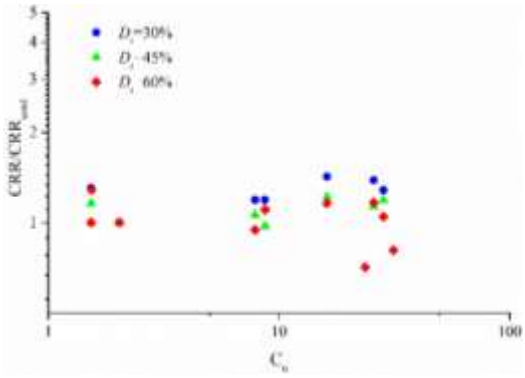

(a) CRR/CRR_{sand} against C_u

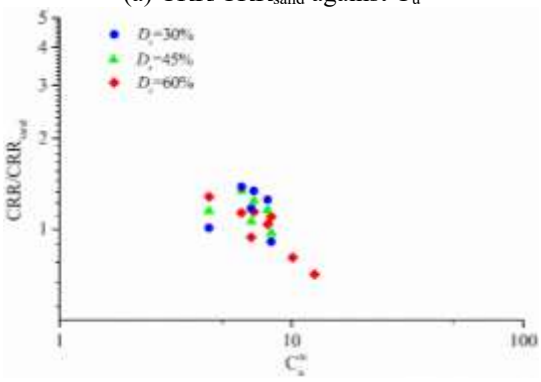

(b) CRR/CRR_{sand} against C_u^m

Fig. 15 The normalized liquefaction resistance CRR/CRR_{sand} of silty sand with respect to C_u and C_u^m

the C_u for the continuous grading. Additionally, the expectation of a decrease trend of e with C_u^m further demonstrates that the proposed new index C_u^m is reasonable.

When the C_u^m, CN_m, G_p and σ_0 are given, the G_0 of granular mixtures can be predicted based on the Eq. (3), which is similar with that of the continuous grading (see Eq. (1)).

4. Discussion and limitation

Based on the above findings, C_u^m is introduced to capture the combined influence of PSR and FC on the packing efficiency and contact structure of gap-graded mixtures. A higher C_u^m reflects more efficient void filling by finer particles, leading to a denser and more more stable

fabric, whereas a lower C_u^m indicates less effective filling and a more open, unstable structure. This interpretation enables C_u^m to be directly linked to the evolution of void ratio and coordination number, which are fundamental indicators of soil mechanical behavior. The well application of the proposed index C_u^m could be found for the liquefaction resistance analysis of gap-graded granular mixtures under cyclic loading. Past case histories of earthquake-induced liquefaction have shown that they are frequently implicated in liquefaction failures (Monkul *et al.* 2021, Banerjee *et al.* 2023). Traditionally, the cyclic resistance ratio (CRR) has been employed to evaluate the liquefaction resistance of soils through cyclic shear tests.

To highlight the advantage of C_u^m over the conventional parameter C_u, Figs. 15(a) and 15(b) illustrate the normalized liquefaction resistance, expressed as CRR/CRR_{sand}, of silty sand with respect to C_u and C_u^m, respectively, where CRR_{sand} denotes the CRR of clean sand. The data points in Figs. 15(a) and 15(b) were obtained from Monkul *et al.* (2021) by digitizing the relevant CRR graphs, which include variations in fines content (FC) and relative density information (D_r). From Fig. 15(a), it can be observed that with increasing C_u, the normalized CRR fluctuates within a certain range across different D_r values. The data points appear scattered and no consistent trend emerges. This observation is in line with previous studies on the effect of gradation, where no systematic relationship could be established between C_u and CRR, even for silty sands (Belkhatir *et al.* 2011). In contrast, Fig. 15(b) shows that the data points are more concentrated, and the normalized CRR exhibits a clear monotonic decrease with increasing C_u^m. This trend is consistent with earlier findings for clean sands, where liquefaction resistance was found to gradually decrease with increasing C_u. These results suggest that, although C_u^m is derived through numerical simulations and data fitting, it serves a more reliable parameter than the traditional C_u for characterizing the heterogeneity and mechanical behavior of gap-graded granular mixtures. In this study, spherical particles were adopted to isolate the effects of fines content (FC) and particle size ratio (PSR) while maintaining computational efficiency. Nevertheless, it should be noted that realistic particle shape features, such as angularity and surface roughness, can significantly influence particle crushing, coordination number, and stiffness evolution (Zhou *et al.* 2013, Ru *et al.* 2017, Gong *et al.* 2025). The influence of particle shape will be investigated in further work.

5. Conclusions

The traditional uniformity coefficient C_u cannot reflect the uniformity of gap-graded granular mixtures. This paper proposes a new index C_u^m, that can be expressed of fines content (FC) and particle size ratio (PSR), to quantify the uniformity of granular mixtures. To obtain C_u^m, the small-strain stiffness G_0 of granular mixtures with different FCs and PSRs are studied. The G_0 values are determined by a quasistatic drained triaxial test. The results show that the evolutions of G_0 with FC follow the similar development for different PSRs. Specifically, with a continuously increase of FC, G_0 first decreases and reaches a valley at FC=20%, then reversely increases and reaches a peak at a specific FC, and finally decreases until FC=100%. The valley G_0 decreases and the peak G_0 increases with an increase of PSR. Assuming that the empirical expression (Eq. (1)) also holds true for predicting the G_0 of granular mixtures after replacing the C_u with C_u^m. Afterwards, C_u^m is calculated based on the measured G_0 values. By fitting the obtained C_u^m values, C_u^m can then be expressed as a function of FC and PSR. The rationality of the proposed C_u^m is verified through two aspects. On the one hand, the proposed C_u^m is used to predict the G0 of granular mixtures with PSR=9.0. The result indicates that the prediction of $G_0/\sigma_0^{1/3}$ compares well with the measured values. On the other hand, the relationship between void ratios e of granular mixtures and C_u^m is validated, together with the data of continuous grading. As expected, for both continuous grading and gap-graded granular mixtures, the measured e monotonically decreases with an increase of C_u^m. The C_u^m can be used to predict the G_0 of granular mixtures when the mechanical coordination number (CN_m), shear modulus of particles (G_p), confining stress (σ_0) and C_u^m are given.

Acknowledgments

The authors would also like to express their appreciation for the financial assistance. This research was financially supported by the National Natural Science Foundation of China (No. 52368045), the Guangxi Natural Science Foundation (No. 2024JJA160220), Fundamental Research Funds for the Central Universities (22120250469) and Shanghai Rising-Star Program (No. 23YF1449100). The authors express their appreciation for the financial assistance.

References

Abbireddy, C.O.R. and Clayton, C.R.I. (2010), "Varying initial void ratios for dem simulations", *Géotechnique*, **60**(6), 497-502. https://doi.org/10.1680/geot.2010.60.6.497.

Azema, E. and Radjai, F. (2010), "Stress-strain behavior and geometrical properties of packings of elongated particles", *Phys Rev E Stat Nonlin Soft Matter Phys*, **81**(5), 51304. https://doi.org/10.1103/PhysRevE.81.051304.

Azéma, E., Radjai, F. and Dubois, F. (2013), "Packings of irregular polyhedral particles: strength, structure, and effects of angularity", *Physical Review. E, Statistical, Nonlinear, and Soft Matter Physics*, **87**(6), 62203. https://doi.org/10.1103/PhysRevE.87.062203.

Banerjee, S.K., Yang, M. and Taiebat, M. (2023), "Effect of coefficient of uniformity on cyclic liquefaction resistance of granular materials", *Comput. Geotech.*, **155**, 105232. https://doi.org/10.1016/j.compgeo.2022.105232.

Belkhatir, M., Arab, A., Schanz, T., Missoum, H. and Della, N. (2011), "Laboratory study on the liquefaction resistance of sand-silt mixtures: effect of grading characteristics", *Granul. Matter.*, **13**(5), 599-609. https://doi.org/10.1007/s10035-011-0269-0.

Chang, D.S., Zhang, L.M., Xu, Y. and Huang, R.Q. (2011), "Field testing of erodibility of two landslide dams triggered by the 12

may wenchuan earthquake", *Landslides*, **8**(3), 321-332. https://doi.org/10.1007/s10346-011-0256-x.

Chen, G., Wu, Q., Zhao, K., Shen, Z. and Yang, J. (2020), "A binary packing material–based procedure for evaluating soil liquefaction triggering during earthquakes", *J. Geotech. Geoenviron. Eng.*, **146**(6), 4020040. https://doi.org/10.1061/(ASCE)GT.1943-5606.0002263.

Cheng, K., Zhang, J., Miao, Y., Ruan, B. and Peng, T. (2019), "The effect of plastic fines on the shear modulus and damping ratio of silty sands", *Bull. Eng. Geol. Environ.*, **78**(8), 5865-5876. https://doi.org/10.1007/s10064-019-01522-1.

Choo, H. and Burns, S.E. (2015), "Shear wave velocity of granular mixtures of silica particles as a function of finer fraction, size ratios and void ratios", *Granul. Matter.*, **17**(5), 567-578. https://doi.org/10.1007/s10035-015-0580-2.

Do, T., Laue, J., Mattsson, H. and Jia, Q. (2024), "Migration of fine granular materials into overlying layers using a modified large-scale triaxial system", *Geomech. Eng.*, **37**(4), 359-370. https://doi.org/10.12989/gae.2024.37.4.359.

Dutta, T.T., Otsubo, M., Kuwano, R. and O'Sullivan, C. (2019), "Stress wave velocity in soils: apparent grain-size effect and optimum input frequencies", *Géotechnique Lett.*, **9**(4), 340-347. https://doi.org/10.1680/jgele.18.00219.

Gong, J., Cheng, L., Zhao, L., Zou, J., Li, L. and Nie, Z. (2021), "Study on the packing and shear characteristics of granular mixtures via the DEM", *Geomech. Eng.*, **27**(3), 223-237. https://doi.org/10.12989/gae.2021.27.3.223.

Gong, J., Li, L., Zhao, L., Zou, J. and Nie, Z. (2021), "Dem study on effects of fabric and aspect ratio on small strain stiffness of granular soils", *Geomech. Eng.*, **24**(1), 57-65. http://doi.org/10.12989/gae.2021.24.1.057.

Gong, J., Nie, Z., Zhu, Y., Liang, Z. and Wang, X. (2019), "Exploring the effects of particle shape and content of fines on the shear behavior of sand-fines mixtures via the dem", *Comput. Geotech.*, **106**, 161-176. https://doi.org/10.1016/j.compgeo.2018.10.021.

Gong, J., Pang, X., Tang, Y., Liu, M., Jiang, J. and Ou, X. (2024), "Effects of particle shape, physical properties and particle size distribution on the small-strain stiffness of granular materials: A dem study", *Comput. Geotech.*, **165**, 105903. https://doi.org/10.1016/j.compgeo.2023.105903.

Gong, J., Wang, X., Li, L. and Nie, Z. (2019), "Dem study of the effect of fines content on the small-strain stiffness of gap-graded soils", *Comput. Geotech.*, **112**, 35-40. https://doi.org/10.1016/j.compgeo.2019.04.008.

Gong, J., Li, Z.Y., Nie, J.Y., Cui, Y.F., Jiang, J. and Ou X.D., (2025), "Study on the automated characterization of particle size and shape of stacked gravelly soils via deep learning", *Acta Geotech.*, **20**, 2369-2394. https://doi.org/10.1007/s11440-024-02493-8.

Goudarzy, M., König, D. and Schanz, T. (2016), "Small strain stiffness of granular materials containing fines", *Soils Found.*, **56**(5), 756-764. https://doi.org/10.1016/j.sandf.2016.08.002.

Goudarzy, M., Magnanimo, V., König, D. and Schanz, T. (2020), "Anisotropic stress state and small strain stiffness in granular materials: rc experiments and dem simulations", *Meccanica*, **55**(10), 1869-1883. https://doi.org/10.1007/s11012-020-01229-8.

Gu, X. and Yang, S. (2018), "Why the ocr may reduce the small strain shear stiffness of granular materials?", *Acta Geotech.*, **13**(6), 1467-1472. https://doi.org/10.1007/s11440-018-0695-9.

Gu, X., Liang, X., Shan, Y., Huang, X. and Tessari, A. (2020), "Discrete element modeling of shear wave propagation using bender elements in confined granular materials of different grain sizes", *Comput. Geotech.*, **125**, 103672. https://doi.org/10.1016/j.%20compgeo.2020.103672.

Gu, X., Lu, L. and Qian, J. (2017), "Discrete element modeling of the effect of particle size distribution on the small strain stiffness of granular soils", *Particuology*, **32**, 21-29. https://doi.org/10.1016/j.partic.2016.08.002.

Gu, X.Q. and Yang, J. (2013), "A discrete element analysis of elastic properties of granular materials, Granul", *Matter*, **15**(2), 139-147. https://doi.org/10.1007/s10035-013-0390-3.

Itasca Consulting Group, Inc. (2014), User's Manual for PFC3D, Minneapolis, USA.

Krishna, P. and Pandey, D. (1981), "5 Close-Packed Structures", First Series Pamphlets No. 5; International Union of Crystallography Commission on Crystallographic Teaching.

Kristiansen, K.D.L., Wouterse, A. and Philipse, A. (2005), "Simulation of random packing of binary sphere mixtures by mechanical contraction", *Physica a: Statistical Mechanics and its Applications*, **358**(2-4), 249-262. https://doi.org/10.1016/j.physa.2005.03.057.

Liu, X., Li, Z., Zou, D., Sun, L., Yahya, K.E. and Liang, J. (2023), "Improving the prediction accuracy of small-strain shear modulus of granular soils through psd: an investigation enabled by dem and machine learning technique", *Comput. Geotech.*, **157**, 105355. https://doi.org/10.1016/j.compgeo.2023.105355.

Liu, X., Yang, J., Zou, D., Li, Z., Chen, Y. and Cao, X. (2024), "Utilizing dem and interpretable ml algorithms to examine particle size distribution's role in small-strain shear modulus of gap-graded granular mixtures", *Constr. Build. Mater.*, **428**, 136232. https://doi.org/10.1016/j.conbuildmat.2024.136232.

Liu, X., Zou, D., Liu, J. and Zheng, B. (2021), "Predicting the small strain shear modulus of coarse-grained soils", *Soil Dyn. Earthq. Eng.*, **141**, 106468. https://doi.org/10.1016/j.soildyn.2020.106468.

Monkul, M.M., Kendir, B.S., Tutuncu, E.Y. (2021), "Combined effect of fines content and uniformity coefficient on cyclic liquefaction resistance of silty sands", *Soil Dyn. Earthq. Eng.*, **151**, 106999. https://doi.org/10.1016/j.soildyn.2021.106999.

Meng, L., Lu, P. and Li, S. (2014), "Packing properties of binary mixtures in disordered sphere systems", *Particuology*, **16**, 155-166. https://doi.org/10.1016/j.partic.2014.02.010.

Nie, J., Shi, X., Cui, Y. and Yang, Z. (2022), "Numerical evaluation of particle shape effect on small strain properties of granular soils", *Eng. Geol.*, **303**, 106652. https://doi.org/10.1016/j.enggeo.2022.106652.

Otsubo, M. and O'Sullivan, C. (2018), "Experimental and dem assessment of the stress-dependency of surface roughness effects on shear modulus", *Soils Found.*, **58**(3), 602-614. https://doi.org/10.1016/j.sandf.2018.02.020.

Otsubo, M., Liu, J., Kawaguchi, Y., Dutta, T.T. and Kuwano, R. (2020), "Anisotropy of elastic wave velocity influenced by particle shape and fabric anisotropy under k condition", *Comput. Geotech.*, **128**, 103775. https://doi.org/10.1016/j.compgeo.2020.103775.

Papadopoulou, A. and Tika T. (2008), "The effect of fines on critical state and liquefaction resistance characteristics of non-plastic silty sands", *Soils Found.*, **48**(5), 713-725. https://doi.org/10.3208/sandf.48.713.

Pinson, D., Zou, R.P., Yu, A.B., Zulli, P. and Mccarthy, M.J. (1998), "Coordination number of binary mixtures of spheres", *J. Physics D: Appl. Phys.*, **31**, 457-462. http://doi.org./10.1088/0022-3727/31/4/016.

Polito, C.P. and Martin, I.J.R. (2001), "Effects of nonplastic fines on the liquefaction resistance of sands", *J. Geotech. Geoenviron. Eng.*, **127**(5), 408-415. https://doi.org/10.1061/(ASCE)1090-0241(2001)127:5(408).

Rahman, M.M. and Lo, S.R. (2014), "Undrained behavior of sand-fines mixtures and their state parameter", *J. Geotech. Geoenviron. Eng.*, **140**(7). https://doi.org/10.1061/(ASCE)GT.1943-5606.0001115.

Ru, F., Hu, X.L. and Zhou, B. (2017), "Discrete element modeling

of crushable sands considering realistic particle shape effect", *Comput. Geotech*., **91**, 179-191. http://dx.doi.org/10.1016/j.compgeo.2017.07.016.

Ruan, B., Miao, Y., Cheng, K. and Yao, E. (2021), "Study on the small strain shear modulus of saturated sand-fines mixtures by bender element test", *Eur. J. Environ. Civ. Eng*., **25**(1), 28-38. https://doi.org/10.1080/19648189.2018.1513870.

Sandeep, C. and Senetakis, K. (2018), "Effect of young's modulus and surface roughness on the inter-particle friction of granular materials", *Materials*, **11**(2), 217. http://doi.org/10.3390/ma11020217.

Sandeep, C.S. and Senetakis, K. (2019), "An experimental investigation of the microslip displacement of geological materials", *Comput. Geotech*., **107**, 55-67. https://doi.org/10.1016/j.compgeo.2018.11.013.

Sefi, F. and Lav, M.A. (2023), "One-dimensional compression behavior of granular soils around virgin compression line (vcl)", *Bull. Eng. Geol. Environ*., **82**(6). https://doi.org/10.1007/s10064-023-03229-w.

Shin, B. (2018), "Laboratory investigation of the stiffness and damping properties of binary and gap-graded mixtures of granular soils", Ph.D. Dissertation, The University of Texas at Austin, Austin.

Thevanayagam, S., Shenthan, T., Mohan, S. and Liang, J. (2002), "Undrained fragility of clean sands, silty sands, and sandy silts", *J. Geotech. Geoenviron. Eng.*, **128**(10), 849-859. https://doi.org/10.1061/(ASCE)1090-0241(2002)128:10(849).

Thornton, C. (2000), "Numerical simulations of deviatoric shear deformation of granular media", *Géotechnique*, **50**(1), 43-53. https://doi.org/10.1680/geot.2000.50.1.43.

Wang, J. and Yan, H. (2012), "Dem analysis of energy dissipation in crushable soils", *Soils Found*., **52**(4), 644-657. https://doi.org/10.1016/j.sandf.2012.07.006.

Wang, T., Wautier, A., Liu, S. and Nicot, F. (2022), "How fines content affects granular plasticity of under-filled binary mixtures", *Acta Geotech*., **17**(6), 2449-2463. https://doi.org/10.1007/s11440-021-01430-3.

Wei, L.M. and Yang, J. (2014), "On the role of grain shape in static liquefaction of sand–fines mixtures", *Géotechnique*, **64**(9), 740-745. https://doi.org/10.1680/geot.14.T.013.

Wei, X. and Yang, J. (2019), "Cyclic behavior and liquefaction resistance of silty sands with presence of initial static shear stress", *Soil Dyn. Earthq. Eng*., **122**, 274-289. https://doi.org/10.1016/j.soildyn.2018.11.029.

Wichtmann, T. and Triantafyllidis, T. (2009), "Influence of the grain-size distribution curve of quartz sand on the small strain shear modulus gmax", *J. Geotech. Geoenviron. Eng*., **135**(10), 1404-1418. https://doi.org/10.1061/(ASCE)GT.1943-5606.0000096.

Yang, J. and Liu, X. (2016), "Shear wave velocity and stiffness of sand: the role of non-plastic fines", *Géotechnique*, **66**(6), 500-514. http://dx.doi.org/10.1680/jgeot.15.P.205.

Yilmaz, Y., Deng, Y., Chang, C.S. and Gokce, A. (2023), "Strength–dilatancy and critical state behaviours of binary mixtures of graded sands influenced by particle size ratio and fines content", *Géotechnique*, **73**(3), 202-217. https://doi.org/10.1680/jgeot.20.P.320.

Youd, T.L. (1972), "Compaction of sands by repeated shear straining", *J. Soil Mech. Found. Div.*, **98**(7), 709-725.

Yu, A.B. and Standish, N. (1988), "An analytical—parametric theory of the random packing of particles", *Powder Technol*., **55**(3), 171-186. https://doi.org/10.1016/0032-5910(88)80101-3.

Zhou, B., Huang, R.Q., Wang, H.B. and Wang, J.F. (2013), "DEM investigation of particle anti-rotation effects on the micromechanical response of granular materials", *Powder Technol*., **15**, 315-326. https://doi.org/10.1007/s10035-013-0409-9.

Zhao, J., Zhao, S. and Luding, S. (2023), "The role of particle shape in computational modelling of granular matter", *Nat. Rev. Phys*., **5**(9), 505-525. https://doi.org/10.1038/s42254-023-00617-9.

Zheng, Y., Bu, J.T., Nie, J.Y. and Liu, Z.Y. (2025), "DEM insights into shear strength weakening mechanism of granular material under high-frequency vibration load", *Comput Geotech*., **181**, 107609. https://doi.org/10.1016/j.compgeo.2025.107609.

Zhu, Y., Gong, J. and Nie, Z. (2020), "Numerical investigation of the elastic properties of binary mixtures as a function of the size ratio and fines content", *Int. J. Geomech*., **20**(9), 4020155. https://doi.org/10.1061/(ASCE)GM.1943-5622.0001792.

Zuo, K., Gu, X., Zhang, J. and Wang, R. (2023), "Exploring packing density, critical state, and liquefaction resistance of sand-fines mixture using dem", *Comput. Geotech*., **156**, 105278. https://doi.org/10.1016/j.compgeo.2023.105278.

IC